

# A SPARSITY-BASED SIMPLIFICATION METHOD FOR SEGMENTATION OF SPECTRAL-DOMAIN OPTICAL COHERENCE TOMOGRAPHY IMAGES

William Meiniel<sup>a,b</sup>, Yu Gan<sup>c</sup>, Jean-Christophe Olivo-Marin<sup>a</sup>, and Elsa Angelini<sup>b,d</sup>

<sup>a</sup>Institut Pasteur, BioImage Analysis Unit, CNRS UMR 3691, France

<sup>b</sup>LTCI, Telecom Paris, Universite Paris-Saclay, France

<sup>c</sup>Department of Electrical Engineering, Columbia University, New York, NY, USA

<sup>d</sup>ITMAT Data Science Group, NIHR Imperial BRC, CSM, Department of Surgery and Cancer, Faculty of Medicine, Imperial College London, UK

## ABSTRACT

Optical coherence tomography (OCT) has emerged as a promising image modality to characterize biological tissues. With axio-lateral resolutions at the micron-level, OCT images provide detailed morphological information and enable applications such as optical biopsy and virtual histology for clinical needs. Image enhancement is typically required for morphological segmentation, to improve boundary localization, rather than enrich detailed tissue information. We propose to formulate image enhancement as an image simplification task such that tissue layers are smoothed while contours are enhanced. For this purpose, we exploit a Total Variation sparsity-based image reconstruction, inspired by the Compressed Sensing (CS) theory, but specialized for images with structures arranged in layers. We demonstrate the potential of our approach on OCT human heart and retinal images for layers segmentation. We also compare our image enhancement capabilities to the state-of-the-art denoising techniques.

Keywords : Optical Coherence Tomography, Sparse sampling, Image simplification, Image segmentation.

## 1. INTRODUCTION

Optical coherence tomography (OCT) is one of the most promising imaging techniques to characterize biological tissues. Recent techniques like spectral-domain optical coherence tomography (SD-OCT)<sup>1</sup> and swept source optical coherence tomography (SS-OCT)<sup>2</sup> have improved the overall quality of images, both in terms of signal to noise ratio (SNR) and real-time performance. OCT images with higher resolution give access to more details on the morphological and tissue information, broadening the image analysis possibilities in fields like optical biopsy and virtual histology. However, in some specific applications, such as data transmission and segmentation of biological tissues, the large data size can affect the efficiency and effectiveness of data analysis. For instance, a modern ultra-high resolution SD-OCT image over a field of view of  $4mm \times 4mm$  may generate up to 2 GB during data acquisition<sup>3</sup> and the data size is even larger using SS-OCT.

In this work we focus on *in-vitro* SD-OCT images of cardiac and retinal samples, as well as their segmentation. In both cases, tissues are organized in layers, and a large portion of OCT data is redundant while corrupted by speckle noise. A data simplification scheme, targeting data size reduction and denoising via image re-sampling is proposed to make tissue layers extraction simpler and faster, while also enabling data storage reduction. This constitutes a radically different approach from the trend in retinal OCT imaging to design specialized layer segmentation methods such as<sup>4-6</sup> which might not work on pathological cases, require careful parameter tuning (e.g. *a priori* layer thickness information) and sometimes rely on machine-learning.

Inspired by the Compressed Sensing (CS) theory,<sup>7</sup> we propose an image simplification method that exploits the sparsity of structural details in OCT images. Indeed, we are interested in the layer structures of the studied images, and not in details inside the layers. The concept of exploiting the sparsity of SD-OCT images was used for denoising in<sup>8</sup> and more recently in,<sup>9</sup> where segmentation results rely on a dictionary-learning approach, resulting in a long running time when training on high SNR images. The use of Compressed Sensing in SD-OCT has been previously investigated in,<sup>10,11</sup> where the authors proved that it is possible to reconstruct OCT images

using only a fraction of the CCD camera pixels. Their method exploited 1D-Fourier transforms of the acquisition samples, but did not exploit the 2D regularity of the layers. In addition, their method aimed at reconstructing the exact image, and was only tested on noise-free data. Another approach has been proposed by<sup>12</sup>, but their mathematical formulation is not related to Compressed Sensing (CS), as requirements like matrices incoherence<sup>13</sup> are not met in their work.

Compressed Sensing was introduced in<sup>7</sup> and<sup>13</sup>. This theory provides solutions to the ill-posed problem of recovering a signal of interest  $x \in \mathbb{C}^N$  from an observation vector  $y = \Phi x + n \in \mathbb{C}^M$  degraded by an additive noise  $n$  such that  $\|n\|_2 \leq \epsilon$ , in the case where the number  $M$  of linear projections is significantly smaller than the size  $N$  of the signal.<sup>14</sup> To compensate for the indeterminacy, two assumptions must be made: first, the observation operator  $\Phi$  needs to preserve the energy of the signal, up to a controlled error,<sup>14</sup> second, the signal has to be almost sparse in some known dictionary  $\Psi$  (called the sparsifying transform). If the constraints are met, an estimator  $\hat{x}$  of  $x$  is defined as the solution of a convex optimization problem.

In this study, our objective is to simplify SD-OCT myocardial images while preserving detailed information on the layers interfaces toward tissue segmentation. The approach consists in generating a simplified estimator  $\hat{x}$  of the true image  $x$ , from a noisy observation  $y = \Phi x$ , by enhancing piecewise constant areas in the image. The sparsity of the estimator is enforced via minimization of the Total-Variation (TV) norm:<sup>15</sup>  $\|x\|_{\text{TV}} = \sum_{p,q} \sqrt{\partial_h x(p,q)^2 + \partial_v x(p,q)^2}$  where  $\partial_h x$  and  $\partial_v x$  are the partial horizontal and vertical derivatives of the image  $x$ , and  $p, q$  are the pixels coordinates.

## 2. SPARSITY-BASED ADAPTIVE SIMPLIFICATION

Introduced in<sup>16</sup> for denoising, our approach uses multiple CS-based estimations of the acquired noisy image, enforcing TV-sparse piecewise constant layers and horizontal contours via dedicated random sampling patterns in the Fourier domain.

We generate several measurement vectors  $y_k$ , ( $k = 1, \dots, R$ ) by under-sampling the Fourier Transform of the acquired image  $y$ . We then recover partial estimators  $\hat{x}_k$  that we aggregate, computing their pixelwise mean map  $\hat{x}_{\text{mean}}$  and variance map  $\sigma_x$ . Finally, we adaptively combine the mean estimator and a filtered version of the noisy image  $y$ , along the structures enhanced by the variance map.

### 2.1 Implementation

The proposed simplification method is decomposed into four steps: (See Fig.1)

- *Generation of random subsets of measurement vectors  $y_k$  in the Fourier domain:* The OCT images that we want to simplify have a very specific structure, displaying horizontal and almost parallel layers of tissue. We exploit this *a priori* information by using a star-shaped pattern as the sampling operator  $\Phi$  in the Fourier domain (see<sup>17</sup>). To make sure that the principal direction of the layers is recovered, we run a first set of reconstructions using a uniform random sampling, and compute the Hough transform<sup>18</sup> on the resulting variance map (See eq.(3)). From the Hough accumulator we select the main line direction, independently of its position. This direction corresponds to a line of the star pattern. In practice, the principal direction of the layers in the Fourier domain is better recovered by an area slightly thicker than a line. Hence, if we denote by  $\theta$  the angle of the principal line direction obtained with the Hough transform, we sample all angle values within the cone  $\theta \pm \theta_\epsilon$ , with  $\theta_\epsilon = \frac{\pi}{16}$ .

To capture additional local details on the layer interfaces, we complete the Fourier sampling mask with  $N_b = 16$  branches positioned at regular angular intervals in  $2\pi$ . Randomness between  $\Phi_k$  draws on the same image is added via a set of  $N_p$  random coefficients uniformly sampled in the Fourier domain, so that the overall sampling rate is  $\tau\%$ .

- *Reconstruction of partial estimators  $\hat{x}_k$  through convex optimization:*

We solve for ( $k = 1, \dots, R$ ) the classic convex optimization problem based on TV minimization, using NESTA algorithm,<sup>19</sup> as proposed in:<sup>7</sup>

$$\hat{x}_k = \arg \min_x \|x\|_{\text{TV}} \quad \text{s.t.} \quad \|\Phi_k x - y_k\|_2 \leq \epsilon \quad (1)$$

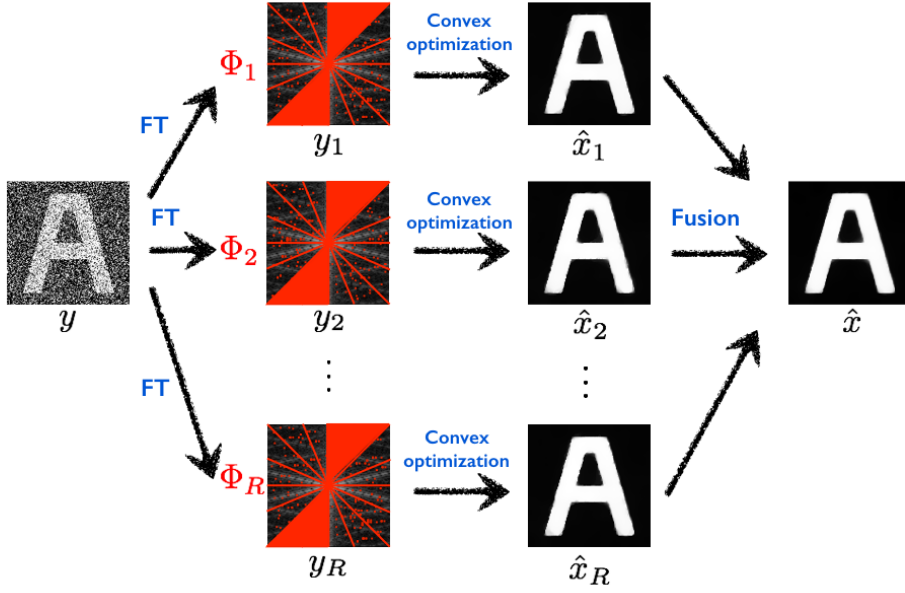


Figure 1: **Image simplification workflow.** From a noisy image  $y$ , a given number of low-sampled measurement vectors  $y_k$  are generated, by taking the Fourier transform of  $y$  and selecting a subset of the Fourier coefficients ( $\Phi_k$ ). Then, each  $y_k$  is used to produce an estimator  $\hat{x}_k$  of the original signal through a convex optimization reconstruction scheme. Finally, all the  $\hat{x}_k$  are combined into an estimator  $\hat{x}$ .

The parameter  $\epsilon$  is defined in<sup>19</sup> to be optimal with respect to the original image, with value:  $\epsilon_0 = \sigma_n \sqrt{\tau N + 2\sqrt{2\tau N}}$  which depends on the estimated noise variance  $\sigma_n$  and the sampling rate  $\tau$ . In this work, we want to enforce TV sparsity, and therefore give more weight to the regularization term than to the data fitting term. The values chosen for  $\epsilon$  depend on the target application, and are detailed in 1. Note that the noise level in the cardiac images is of higher intensity, requiring larger values of  $\epsilon$ .

- *Fusion of the  $\hat{x}_k$  to produce the mean image  $\hat{x}_{\text{mean}}$  and the variance map  $\sigma_x$ :* We aggregate the partial estimators via computation of their mean:

$$\hat{x}_{\text{mean}} = \frac{1}{R} \sum_{k=1}^R \hat{x}_k \quad (2)$$

The fused estimator  $\hat{x}_{\text{mean}}$  provides an estimation of the denoised image, where the constant areas represent the layers of the sample. We also define the variance map of the reconstructions as follows:

$$\sigma_x = \sqrt{\frac{1}{R-1} \sum_{k=1}^R (\hat{x}_k - \hat{x}_{\text{mean}})^2} \quad (3)$$

The map  $\sigma_x$  (illustrated in Fig. 2) reveals edge structures corresponding to dissimilarities between different partial estimators  $\hat{x}_k$ . This map highlights very accurately the separations between different tissue layers of the sample and is less sensitive to local contrast than a standard gradient map.

- *Adaptive reconstruction using fusion with a local filter  $\mathcal{H}$ :* We finally define the simplified enhanced image  $\hat{x}$  as follows:

$$\hat{x} = (1 - \sigma_x) \circ \hat{x}_{\text{mean}} + \sigma_x \circ \mathcal{H}(y) \quad (4)$$

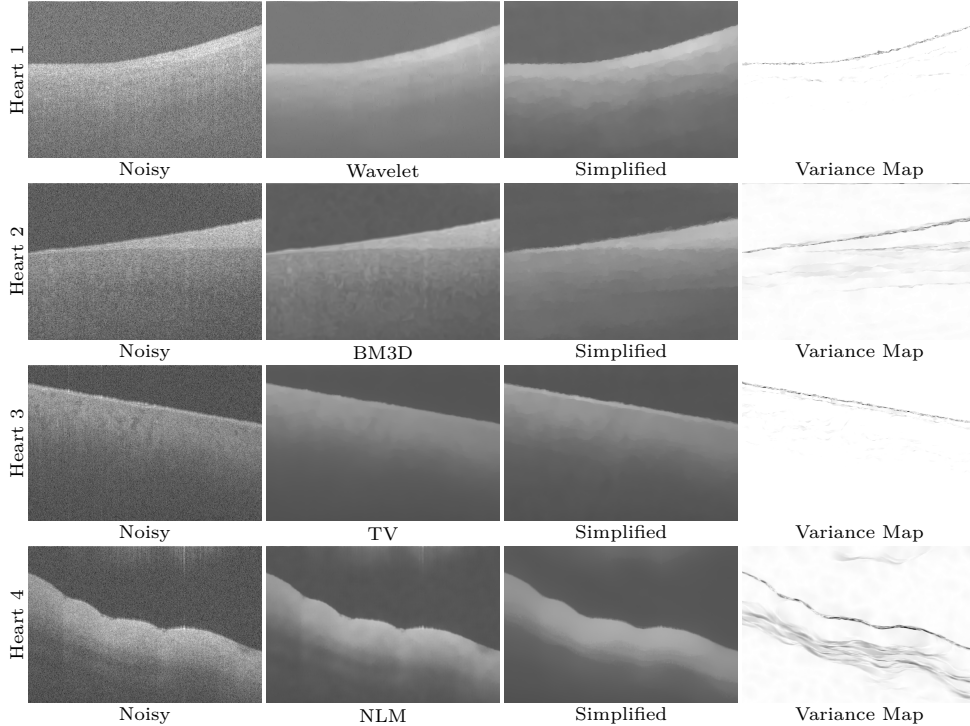


Figure 2: **Simplification of the heart images.** For each noisy data, we present the result of our simplification algorithm, along with one of the 4 tested denoising methods: BM3D, Wavelet soft-thresholding, TV and NLM. See 3.1 for a detailed comparison of the results.

where  $\circ$  is the Hadamard product, and  $\mathcal{H}$  represents a local smoothing filter applied on the original image  $y$ . Here we used a simple  $3 \times 3$  Gaussian filter with variance  $\sigma = 0.06$ .

## 2.2 Parameters setting

See<sup>16</sup> for a complete study of the parameters used for our method. In the specific case of OCT image simplification, a main objective is to reconstruct simplified images using very few Fourier coefficients. We set for all our experiments the sampling rate to  $\tau = 5\%$ , and the number of reconstructions to  $R = 3$ . Overall, only 8.7% of the Fourier coefficients of the noisy image  $y$  are exploited to reconstruct a simplified version  $\hat{x}$  of the original image, since the coefficients of the star Fourier sampling pattern are shared between reconstructions.

## 3. EXPERIMENTAL RESULTS

### 3.1 Experimental Setup

#### 3.1.1 Comparison to state of the art denoising

We compared our image enhancement results to four state of the art methods: TV-filtering,<sup>15</sup> Non-Local Means,<sup>20</sup> Wavelet soft-thresholding<sup>21</sup> (commonly used for OCT-image denoising<sup>22</sup>), and BM3D<sup>23</sup> (which is the reference for most denoising algorithms).

Parameter values for this four methods were empirically set and are listed in Table 1.

#### 3.1.2 OCT data sets

**Cardiac OCT images** We evaluated our algorithm on a set of 4 human hearts (See Fig.2) with the following characteristics:

Table 1: **Parameter values of the different denoising methods.**

Method	Reference	Parameters
TV	15	Cardiac: $\epsilon = 61.12$ , Retinal: $\epsilon = 28.44$
NLM	20	Patch size = $4px$ , $\alpha = 0.1$
Wavelet thresh.	21	$\lambda_{\text{wav}} = 0.2$ , wavelet depth = 10, wavelet type = haar
BM3D	23	$\sigma_b = 75$
Proposed	16	$R = 3$ , $N_b = 16$ , $\tau = 5\%$ , $\epsilon = 13.78$

$px = \text{pixels}$ .

- *Heart 1: One layer of constant thickness.* Such configuration is typical for human atrial tissue, where the regular layer corresponds to dense collagen.
- *Heart 2: One layer of non-constant thickness.* Such configuration is typical of a diseased human cardiac tissue. The enlarged dense collagen layer is caused by myocardial scar.
- *Heart 3: One thin layer.* Such configuration is typical for healthy ventricular septum. The thin layer is the endothelium, and there is no dense collagen layer.
- *Heart 4: Two layers.* On some human atrial tissue, we can distinguish deeper layers, beyond the dense collagen in the first layer. They correspond to loose collagen, smooth muscle, or elastic tissues.

**Retinal OCT images** We exploited the data set of retinal OCT images shared by the authors of<sup>24</sup> on the link [http://people.duke.edu/~sf59/Srinivasan\\_B0E\\_2014\\_dataset.htm](http://people.duke.edu/~sf59/Srinivasan_B0E_2014_dataset.htm). This data set was obtained with Institutional Review Board-approved protocols using a Spectralis SD-OCT (Heidelberg Engineering Inc.) imaging system at Duke University. The following population of 45 subjects was screened: 15 healthy subjects, 15 patients with dry age-related macular degeneration (AMD), and 15 patients with diabetic macular edema (DME). In this paper, we focus on the healthy subjects, as they encompass the most challenging cases.

### 3.2 Qualitative evaluation

Regarding the myocardial OCT images, we can observe on Fig.2 that the four state of the art methods lead to visual degradation of image content for at least one case: over-smoothing of one layer (Heart 1, wavelet soft-thresholding; Heart 3, TV filtering), introducing strong visual artifacts such as oscillations (Heart 2 with BM3D; Heart 4 with NLM), patch effects (NLM) and staircasing (TV). Regarding visual quality on fine structural details on individual cases, we can make the following remarks: For the *Heart 1* image, wavelet soft-thresholding fails to detect the lower border of the layer, which impact the segmentation of the dense collagen layer. The image *Heart 2* has a high level of noise which greatly degrades the performance of BM3D. The image *Heart 3* is over-smoothed by TV regularization which leads to disappearance of the thin endothelium layer. The image *Heart 4* is poorly denoised by NLM, with a patchy appearance and the introduction of outliers in the upper part of the image.

Regarding the retinal OCT images, visual illustrations of image enhancement with our proposed method and with BM3D are reported in Fig.3. We can see that the two methods generate quite distinct types of images: BM3D enhances thin contrasted structures but removes all texture while our method preserves some texture.

### 3.3 Segmentation of SD-OCT layers

In the field of OCT image segmentation, the problem of intra-retinal layer extraction has been widely studied in the literature. Either performing a graph-search method,<sup>4</sup> a gradient-based approach<sup>5</sup> or a kernel-based optimization algorithm,<sup>6</sup> efficient segmentation solutions are now used in ophthalmology. In this study, we tested the retinal layer segmentation method from<sup>24</sup> which consists in a first step of denoising with a Gaussian filter, followed by a hierarchical graph-based segmentation of the several layers of tissues, to isolate the different compartments of the retina. In the case of strong noise, the segmentation is prone to errors, especially on healthy subjects. In this study, we tested the segmentation method on the original noisy image with Gaussian denoising and on our enhanced images, without additional denoising. Visual illustrations of the results are displayed on

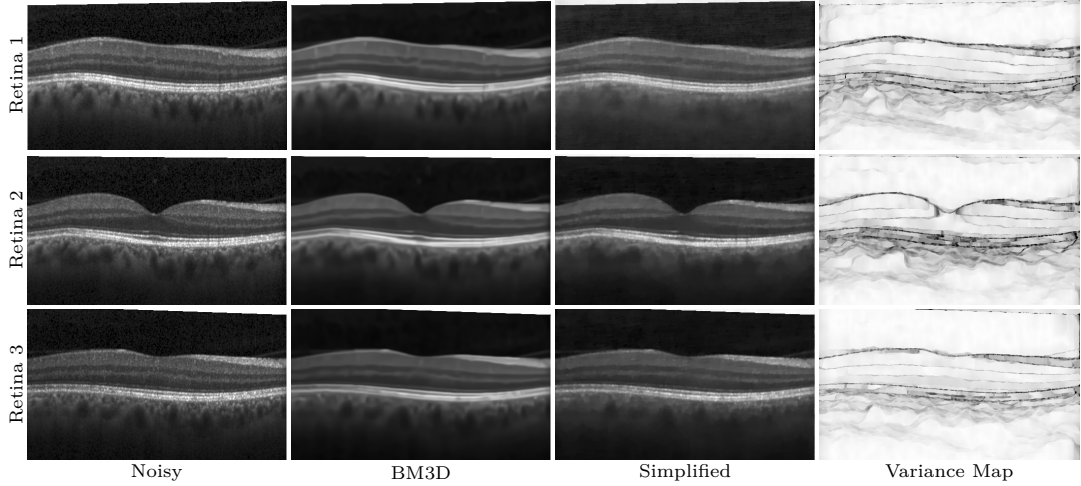


Figure 3: **Simplification of the retinal images.** For each noisy data, we present the result of our simplification algorithm, along with the result given by the BM3D method.

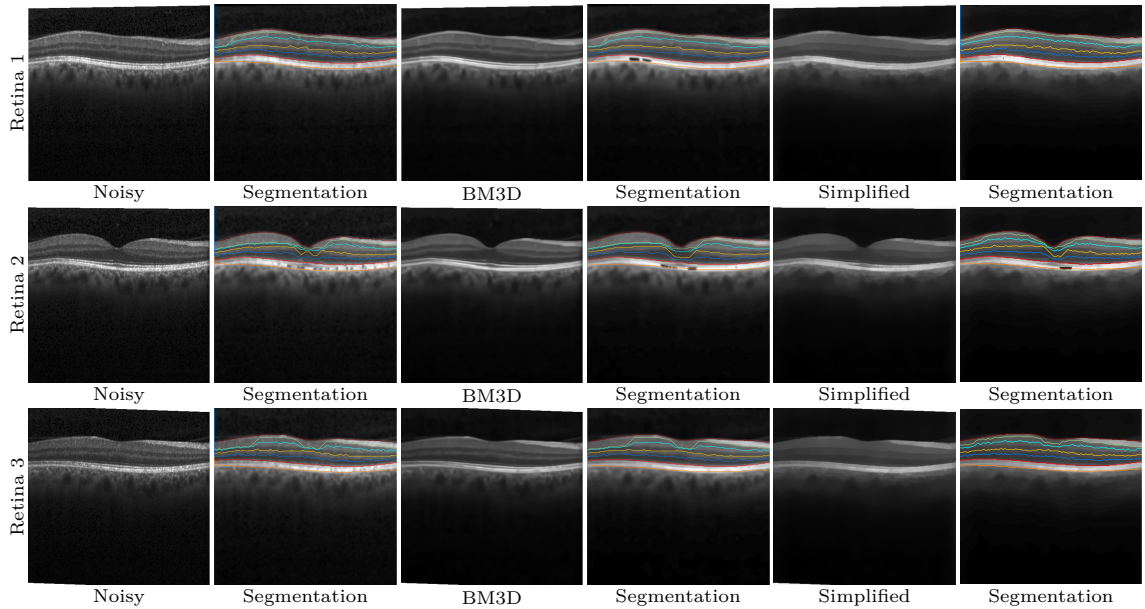


Figure 4: **Simplification and segmentation of the retinal images.** For each noisy data, we present the result of our simplification algorithm, along with the results obtained using the BM3D method. We also display the segmentation result obtained in each case.

Fig. 4. We can see that the segmentation results obtained with our method are comparable to those obtained with the direct method, and after BM3D denoising. Hence, our proposed method only exploiting up to 10% of the measured samples is able to accurately quantify layers which opens a path for efficient image compression.

For the cardiac OCT images, we implemented a sparsity-based segmentation method as follows. The proposed simplification method generates two outputs: the simplified image with layers preserved (in terms of positions and average intensity), and the variance map, with precise delineation of layers interfaces, corresponding to local disagreements between the reconstructions. Segmentation of layers could be performed on either one and we show in Fig. 5 some results exploiting local peak detection on vertical profiles of the variance map. The variance map  $\sigma_x$  of an image  $y$  is the result of the pixelwise variance of the different sparsity-based reconstructions.

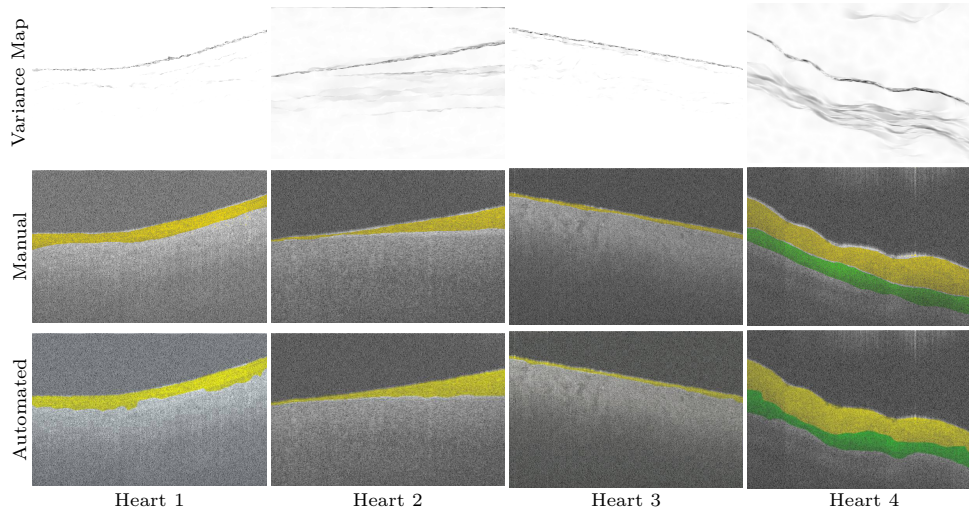


Figure 5: **Segmentation of the heart images.** Variance maps of each heart samples are displayed, along with Manual and Automated segmentation results overlaid on the raw SD-OCT images.

Then, it gives a global information of the local disagreements between the reconstructions. In other words, the variance map is a map of the regions that are not well reconstructed by the TV-based reconstructions methods. These regions are exactly the intersection between the layers of the image (See Fig. 2). We also compared our segmentation results with the manual segmentation from an expert.

#### 4. CONCLUSION

We presented a CS-type Fourier-based image simplification method well suited for the study of layers of tissues on OCT images, and evaluated on retinal or myocardial applications. The proposed method is able to remove noise, preserve tissue layers intensities and positions, and generates a variance map which is directly exploitable for segmentation. A strong benefit of our approach is that it uses less than 10% of the samples in Fourier domain which bears great potentials for data compression. The next step will focus on implementing such image simplification directly at the sensing stage, using multiple CS acquisitions. Such implementation is still not trivial, requiring open OCT systems to modify the sampling scheme and hardware implementation of pseudo-random sampling patterns. In addition *a priori* information such as layer orientations and noise level will need to be inferred prior to acquisition.

#### REFERENCES

- [1] Fercher, A. F., Hitzenberger, C. K., Kamp, G., and El-Zaiat, S. Y., “Measurement of intraocular distances by backscattering spectral interferometry,” *Optics communications* **117**(1-2), 43–48 (1995).
- [2] Chinn, S., Swanson, E., and Fujimoto, J., “Optical coherence tomography using a frequency-tunable optical source,” *Optics letters* **22**(5), 340–342 (1997).
- [3] Yao, X., Gan, Y., Marboe, C. C., and Hendon, C. P., “Myocardial imaging using ultrahigh-resolution spectral domain optical coherence tomography,” *Journal of biomedical optics* **21**(6), 061006–061006 (2016).
- [4] Garvin, M. K., Abramoff, M., Wu, X., Russell, S., Burns, T., and Sonka, M., “Automated 3-D intraretinal layer segmentation of macular spectral-domain optical coherence tomography images,” *IEEE Transactions on Medical Imaging* **28**, 1436–1447 (2009).
- [5] Yang, Q., Reisman, C., Wang, Z., Fukuma, Y., Hangai, M., Yoshimura, N., Tomidokoro, A., Araie, M., Raza, A., Hood, D., and K., C., “Automated layer segmentation of macular OCT images using dual-scale gradient information,” *Opt. Express* **20**(18), 21293–21307 (2010).
- [6] Mishra, A., Wong, A., Bizheva, K., and Clausi, D., “Intra-retinal layer segmentation in optical coherence tomography images,” *Opt. Express* **26**(17), 23719–23728 (2009).

- [7] Candès, E., Romberg, J., and Tao, T., “Robust uncertainty principles: Exact signal reconstruction from highly incomplete frequency information,” *IEEE Transactions on Information Theory* **52**(2), 489–509 (2006).
- [8] Fang, L., Li, S., Nie, Q., Izatt, J., Toth, C., and Farsiu, S., “Sparsity based denoising of spectral domain optical coherence tomography images,” *Biomed. Opt. Express* **3**(5), 927–942 (2012).
- [9] Fang, L., Li, S., Cunefare, D., and Farsiu, S., “Segmentation based sparse reconstruction of optical coherence tomography images,” *IEEE transactions on medical imaging* **36**(2), 407–421 (2017).
- [10] Mohan, N., Stojanovic, I., Karl, W. C., Saleh, B. E., and Teich, M. C., “Compressed sensing in optical coherence tomography,” in [*Proc. SPIE*], **7570**, 75700L (2010).
- [11] Liu, X. and Kang, J. U., “Compressive SD-OCT: the application of compressed sensing in spectral domain optical coherence tomography,” *Optics Express* **18**(21), 22010–22019 (2010).
- [12] Lebed, E., Mackenzie, P. J., Sarunic, M. V., and Beg, M. F., “Rapid volumetric oct image acquisition using compressive sampling,” *Optics express* **18**(20), 21003–21012 (2010).
- [13] Donoho, D., “Compressed sensing,” *Transactions on Information Theory* **52**(4), 1289–1306 (2006).
- [14] Candès, E., “The restricted isometry property and its implications for compressed sensing,” *Comptes Rendus Mathématique* **346**(9 - 10), 589 – 592 (2008).
- [15] Rudin, L. I., Osher, S., and Fatemi, E., “Nonlinear total variation based noise removal algorithms,” *Phys. D* **60**(1-4), 259–268 (1992).
- [16] Meiniel, W., Angelini, E., and Olivo-Marin, J.-C., “Image denoising by adaptive compressed sensing reconstructions and fusions,” in [*Proc. SPIE*], (August 2015).
- [17] Wang, Z. and Arce, G., “Variable density compressed image sampling,” *IEEE Transactions on Image Processing* **19**(1), 264–270 (2010).
- [18] Duda, R. and Hart, P., “Use of the Hough transformation to detect lines and curves in pictures,” *Commun. ACM* **15**(1), 11–15 (1972).
- [19] Becker, S., Bobin, J., and Candès, E., “Nesta: A fast and accurate first-order method for sparse recovery,” *SIAM Journal on Imaging Sciences* **4**(1), 1–39 (2011).
- [20] Buades, A., Coll, B., and Morel, J.-M., “A review of image denoising algorithms, with a new one,” *Multiscale Modeling & Simulation* **4**(2), 490–530 (2005).
- [21] Donoho, D. L., “De-noising by soft-thresholding,” *IEEE Transactions on Information Theory* **41**(3), 613–627 (1995).
- [22] Mayer, M., Borsdorf, A., Wagner, M., Hornegger, J., Mardin, C., and Tornow, R., “Wavelet denoising of multiframe optical coherence tomography data,” *Optics Express* **3**(3), 572–589 (2012).
- [23] Dabov, K., Foi, A., Katkounnik, V., , and Egiazarian, K., “Image denoising by sparse 3D transform-domain collaborative filtering,” *IEEE Transactions on Image Processing* **16**(8), 2080–2095 (2007).
- [24] Srinivasan, P. P., Kim, L. A., Mettu, P. S., Cousins, S. W., Comer, G. M., Izatt, J. A., and Farsiu, S., “Fully automated detection of diabetic macular edema and dry age-related macular degeneration from optical coherence tomography images,” *Biomedical optics express* **5**(10), 3568–3577 (2014).